

Peptide-Reinforced Amphiphilic Polymer Conetworks

Sara T. R. Velasquez, Daseul Jang, Peter Jenkins, Peng Liu, Liu Yang, LaShanda T. J. Korley, and Nico Bruns*

Amphiphilic polymer conetworks (APCNs) are polymer networks composed of hydrophilic and hydrophobic chain segments. Their applications range from soft contact lenses to membranes and biomaterials. APCNs based on polydimethylsiloxane (PDMS) and poly(2-hydroxyethyl acrylate) are flexible and elastic in the dry and swollen state. However, they are not good at resisting deformation under load, i.e., their toughness is low. A bio-inspired approach to reinforce APCNs is presented based on the incorporation of poly(β -benzyl-L-aspartate) (PBLA) blocks between cross-linking points and PDMS chain segments. The mechanical properties of the resulting peptide-reinforced APCNs can be tailored by the secondary structure of the peptide chains (β -sheets or a mixture of α -helices and β -sheets). Compared to non-reinforced APCNs, the peptide-reinforced networks have higher extensibility (53 vs. up to 341%), strength (0.71 ± 0.16 vs. 22.28 ± 2.81 MPa), and toughness (0.10 ± 0.04 vs. up to 4.85 ± 1.32 MJ m⁻³), as measured in their dry state. The PBLA peptides reversibly toughen and reinforce the APCNs, while other key material properties of APCNs are retained, such as optical transparency and swellability in water and organic solvents. This paves the way for applications of APCNs that benefit from significantly increased mechanical properties.

membranes,^[9] antifouling coatings,^[10] and as luminescent solar concentrators for solar cells.^[11] APCNs are two-component polymeric networks containing a hydrophilic and hydrophobic phase, often in a co-continuous nanophase-separated morphology.^[12] Covalent cross-linking prevents macroscopic demixing. Therefore, APCNs are macroscopically homogeneous and optically transparent.^[12c] The ratio of hydrophobic to hydrophilic phase dictates their swelling, permeability and mechanical properties, so that these properties can be tuned by the composition of the monomer feed during polymerization.^[1b,12c] Bruns and co-workers previously synthesized poly(2-hydroxyethyl acrylate)-linked by-polydimethylsiloxane (PHEA-*l*-PDMS) networks as thin coatings and free-standing membranes, finding they were flexible and elastic materials in wet and dry states.^[5a,8,12c,13] However, these and other APCNs have limited stretchability and

often break at low extensions, i.e., they are not tough, which limits their application. Highly stretchable APCNs could be ideal materials, e.g., for biomedical implants, for wound coverings, or for breathable membranes in textiles. However, previous studies have not explored methods to reinforce APCNs in detail.


Polymeric networks that swell in aqueous solvents are hydrogels. Therefore, APCNs are a subclass of hydrogels that also swell in organic solvents.^[1a-d] Conventional polymeric hydrogels display relatively poor mechanical properties, with

1. Introduction

Amphiphilic polymer conetworks (APCNs) are cross-linked polymers that swell in both aqueous and organic solvents due to their molecular structure composed of hydrophilic and hydrophobic chain segments.^[1] Their properties can be tailored to suit a wide range of applications including soft contact lenses,^[2] biomaterials,^[3] drug-delivery materials,^[4] catalyst supports,^[5] sensors,^[6] light-responsive membranes,^[7] self-sealing breathable membranes,^[8] pervaporation and chiral separation

S. T. R. Velasquez, N. Bruns
Department of Pure and Applied Chemistry
University of Strathclyde
Thomas Graham Building, 295 Cathedral Street, Glasgow G1 1XL, UK
E-mail: nico.bruns@tu-darmstadt.de

S. T. R. Velasquez, N. Bruns
Department of Chemistry
Technical University of Darmstadt
Alarich-Weiss-Straße 4, 64287 Darmstadt, Germany

 The ORCID identification number(s) for the author(s) of this article can be found under <https://doi.org/10.1002/adfm.202207317>.

© 2022 The Authors. Advanced Functional Materials published by Wiley-VCH GmbH. This is an open access article under the terms of the Creative Commons Attribution License, which permits use, distribution and reproduction in any medium, provided the original work is properly cited.

DOI: 10.1002/adfm.202207317

D. Jang, L. T. J. Korley
Department of Materials Science and Engineering
University of Delaware
127 The Green, 209 DuPont Hall, Newark, DE 19716, USA

P. Jenkins, L. Yang
Department of Mechanical and Aerospace Engineering
University of Strathclyde
James Weir Building, 75 Montrose Street, Glasgow G1 1XJ, UK

P. Liu
Adolphe Merkle Institute
University of Fribourg
Chemin des Verdiers 4, 1700 Fribourg, Switzerland

L. T. J. Korley
Department of Chemical and Biomolecular Engineering
University of Delaware
150 Academy Street, Newark, DE 19716, USA

strength of ≈ 10 kPa,^[14] in comparison to natural hydrogels such as elastin, resilin and tendon collagen, with strength of 2000, 3000, and 150 000 kPa, respectively.^[15] The low mechanical properties of synthetic hydrogels limit their wider applications and usage.^[16] For example, hydrogels require a strength of ≈ 1000 kPa for continuous load bearing scenarios in, e.g., tissue engineering.^[14b] Other applications where tough hydrogels and, potentially, APCNs are interesting include soft robotics (muscle-like actuators,^[17] electrically assisted actuators,^[18] jelly fish soft robots,^[19] wearable electronics,^[20] tissue engineering,^[21] drug delivery,^[2a] elastomeric materials,^[22] and water evaporation membranes.^[8]

Several methods were used in previous publications to reinforce and toughen hydrogels, including the use of mechanophores that lengthen polymer chains in response to applied forces,^[23] by creating polymer networks with a high concentration of chain entanglements,^[24] the use of ionically and covalently cross-linked networks,^[25] the use of polyzwitterions as building blocks for polymer networks,^[26] and the creation of hierarchical architectures by freezing-assisted salting-out treatment.^[27] Hydrogels that contain hydrophilic and hydrophobic domains, and therefore resemble APCNs, have been successfully reinforced by coupling chemistry,^[28] by the incorporation of nanoparticles,^[29] as nanocomposites through hydrophobic association,^[30] by self-assembly of micelles,^[31] by using star polymers,^[32] and by the formation of interpenetrating,^[33] tetra^[34] or sliding ring^[35] networks. Each approach aimed to improve the mechanical properties of the polymer network by incorporating a secondary mechanism of energy dissipation into the materials. However, most methods to reinforce hydrogels often reduce their stretchability.^[24] Amphiphilic polymer conetworks with very high stretchability have been achieved by incorporating dynamic covalent bonds and triblock copolymer micelles into hydrogels,^[36] and by synthesizing APCNs with PDMS segments separated by PEG segments, in which the hydrophobic interactions of the PDMS segments act as mechanical “fuse link”.^[37]

Some natural materials, including spider silk and collagen, combine both high modulus or yield strength and toughness (energy needed to fracture) that are typically mutually exclusive.^[38] Nature achieves this through hierarchical secondary structures of protein domains that unfold under mechanical load.^[15a,39] Inspired by the toughening mechanisms of natural protein-based materials, some synthetic materials such as polyurethanes or hydrogels reinforced with peptides or proteins have been developed.^[28a,40] For example, ABA triblock copolymers with polyethylene glycol (PEG) or polydimethylsiloxane (PDMS) as the middle B block and poly- β -benzyl-L-aspartate (PBLA) or poly- γ -benzyl-L-glutamate (PBLG) as the A blocks can tune the mechanical properties of polyurethanes.^[40c,e,41] Bioinspired peptide-polymer or protein-polymer hybrids combine the structural hierarchy found in natural materials with synthetic macromolecules to augment mechanical properties.^[40e] The secondary peptide structure determines the thermal and mechanical properties of these materials.^[40c,e,f,42] The intra-molecular hydrogen bonds of α -helices, the inter-chain hydrogen bonds of β -sheets, as well as the hierarchical structures that form in peptides are responsible for the increase in toughness and stiffness of these materials, as the non-covalent

bonds can unravel in response to mechanical forces and reform when the materials relax.^[40a,b,d,43]

Here, we present bioinspired peptide-reinforced APCNs in which hydrophobic crosslinkers, consisting of a central PDMS block and short PBLA homopeptide blocks at each chain end (PBLA-*b*-PDMS-*b*-PBLA triblock copolymers), cross-link hydrophilic PHEA chains. Structurally and chemically, these APCNs resemble the well-established PHEA-*l*-PDMS APCNs, but contain additional peptide blocks between the cross-linking points and the PDMS chain segments. The peptides form, depending on the degree of polymerization of PBLA, β -sheets or a mixture of α -helices and β -sheets. These motifs provide hydrogen bonding and hence reinforcement for energy dissipation, thereby increasing the mechanical properties of the materials. We analyzed in depth the effect of the hydrophobic to hydrophilic ratio and the lengths of the peptide segments on the morphology and the thermal and mechanical properties of the APCNs. The incorporation of the peptidic blocks into the networks resulted in materials with substantially improved strength, failure strain, Young's modulus and toughness.

2. Results and Discussion

2.1. Synthesis of Non-Peptidic and Peptidic Amphiphilic Polymer Conetworks

PHEA-*l*-PDMS APCNs were selected as the base material for this research because they are flexible and elastic in the dry and in the swollen states at room temperature.^[7a] Non-peptidic PHEA-*l*-PDMS samples were prepared as reference materials with a commercial bifunctional α,ω -methacrylate-functionalized PDMS macromonomer (with a number average molecular weight (M_n) of 4500 – 5500 g mol⁻¹ following previous reports.^[5a,12c,44] The peptidic crosslinkers were α,ω -methacrylate functionalized ABA triblock copolymers consisting of a central PDMS block flanked on each side with PBLA blocks (PBLA_{*x*}-*b*-PDMS-*b*-PBLA_{*x*}) of either $x = 5$ or 20 repeating peptide units (**Figure 1A**). As previously reported for polyurea materials using similar PBLA_{*x*}-*b*-PDMS-*b*-PBLA_{*x*} block copolymers,^[40d] the number of BLA repeating units determines the secondary structure of the peptide blocks (**Figure 1B**). Mostly β -sheets were formed when there were less than 10 repeating units and a mixture of β -sheets and α -helix with more than 10 repeating units.^[40d,45] The PBLA_{*x*}-*b*-PDMS-*b*-PBLA_{*x*} block copolymers were prepared by ring opening polymerization of β -benzyl-L-aspartate *N*-carboxyanhydride (BLA-NCA) from a PDMS macroinitiator with NH₂ groups on each chain end and a M_n of 2500 g mol⁻¹. The NCA polymerization yielded α,ω -amine functional block copolymers. They were converted into crosslinkers for radical polymerizations by reacting them with 2-isocyanatoethyl methacrylate, which gave α,ω -methacrylate functionalized MA-PBLA_{*x*}-*b*-PDMS-*b*-PBLA_{*x*}-MA triblock copolymers (**Figure 1A**).

Homogeneous monomer mixtures were achieved by hydrophobically masking the hydrophilic monomer HEA with a trimethylsilyl (TMS) group, as in previous works.^[5a,12c,44] The resulting TMS-HEA was miscible with the PDMS-based and PBLA-*b*-PDMS-*b*-PBLA-based crosslinkers at any ratio.

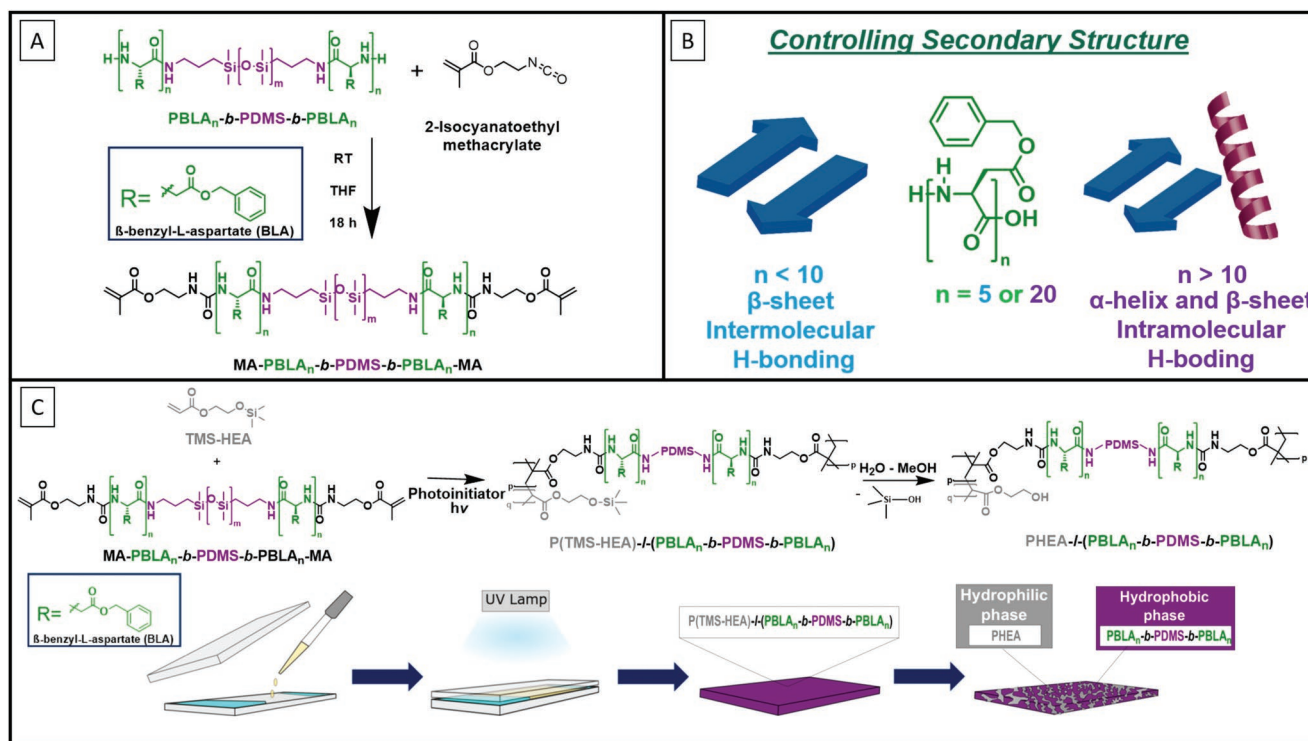


Figure 1. Schematic depiction of the preparation of PHEA-*I*-(PBLA_x-*b*-PDMS-*b*-PBLA_x) APCNs. A) Synthesis procedure for the addition of MA end groups to the PBLA_x-*b*-PDMS-*b*-PBLA_x triblock copolymers. B) Schematic depiction of the influence of the number of BLA repeating units on the secondary structure of the resulting PBLA peptide. C) Reaction scheme and depiction of the APCN preparation procedure.

APCNs were prepared as free-standing films of 150 to 300 μm thickness by UV-induced free radical copolymerization of TMS-HEA/MA-PDMS-MA and TMS-HEA/MA-PBLA_x-*b*-PDMS-*b*-PBLA_x-MA with small quantities of dimethylsulfoxide (DMSO) as solvent (Figure 1C and Table 1). After photopolymerization, hydrophobic precursor networks were obtained. They were converted into APCNs by removal of the TMS-groups, which easily cleaved off when the networks were

swollen overnight in a 50:50 (v:v) isopropanol-water mixture, followed by 4 h in methanol. Samples with different peptide content and HI to HO ratios were prepared. Throughout this work, the materials were labeled as PBLAXX_YY, where XX is the degree of polymerization of the peptide (PBLA00, PBLA05 and PBLA20) and YY is the PHEA wt.% (0, 30, 50 or 70 wt.%), assuming the same molar composition of monomers and macromonomers in the final networks as in the monomer

Table 1. Composition of the APCNs and of the reaction mixtures used to synthesize these APCNs.

Sample	Composition of APCN [% wt]			Composition of monomer mixture [mg]			Initiator [mg]	Solvent DMSO [μl]
	PHEA	PDMS	PBLA _x - <i>b</i> -PDMS- <i>b</i> -PBLA _x	TMS-HEA	MA-PDMS-MA	MA-PBLA _x - <i>b</i> -PDMS- <i>b</i> -PBLA _x -MA		
PBLA00_00	0	100	–	0.0	500	–	3.0	0
PBLA00_30	30	70	–	243.2	350	–	3.6	0
PBLA00_50	50	50	–	405.4	250	–	3.9	0
PBLA00_70	70	30	–	567.6	150	–	4.3	0
PBLA05_00	0	–	100	0.0	–	500	3.0	333
PBLA05_30	30	–	70	243.2	–	350	3.6	233
PBLA05_50	50	–	50	405.4	–	250	3.9	167
PBLA05_70	70	–	30	567.6	–	150	4.3	100
PBLA20_00	0	–	100	0.0	–	500	3.0	667
PBLA20_30	30	–	70	243.2	–	350	3.6	467
PBLA20_50	50	–	50	405.4	–	250	3.9	333
PBLA20_70	70	–	30	567.6	–	150	4.3	200

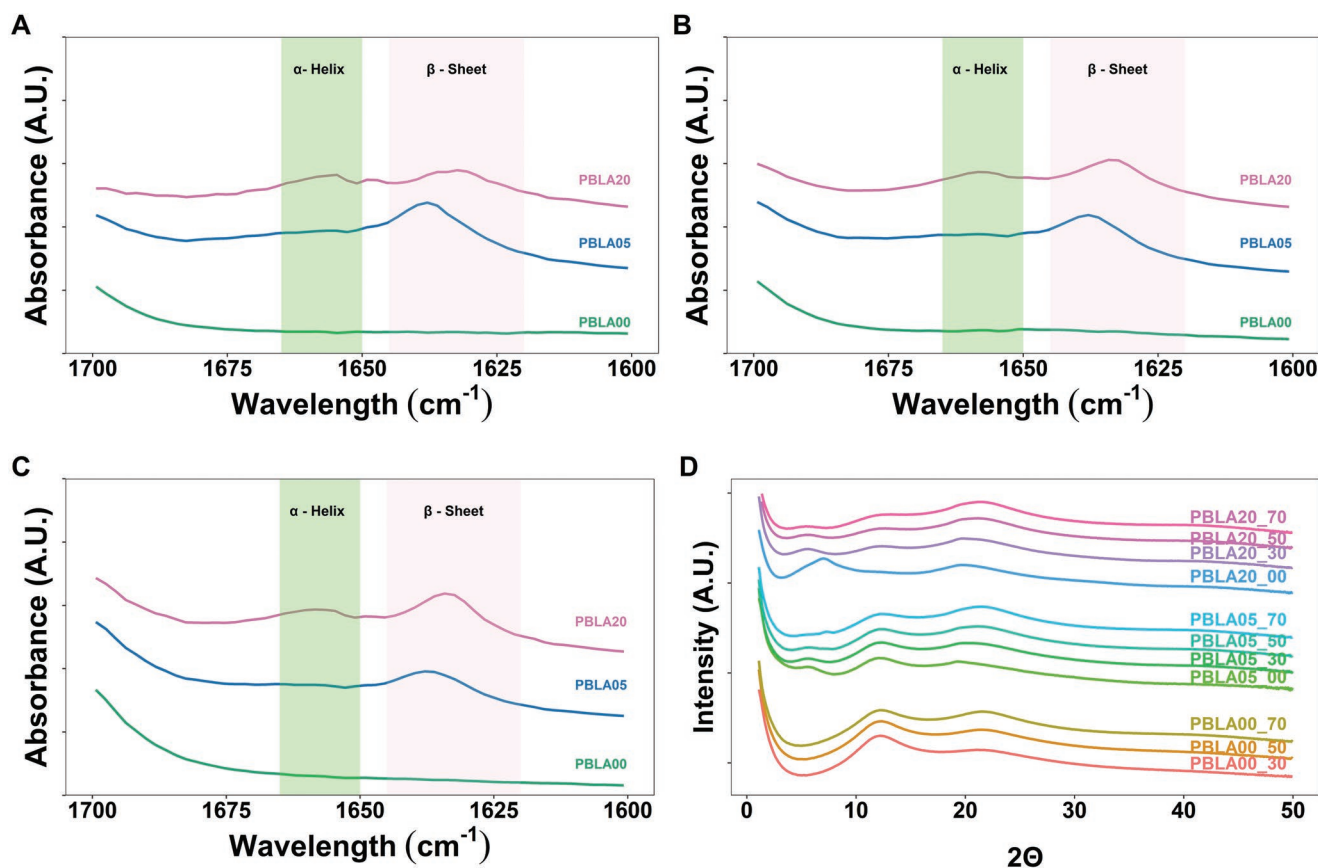


Figure 2. ATR-FTIR spectra of PHEA-*l*-PDMS and PHEA-*l*-(PBLA_{*x*}-*b*-PDMS-*b*-PBLA_{*x*}) APCNs in the amide I region and WAXS data. A) APCNs with 30 wt.% PHEA and different lengths of PBLA blocks. B) APCNs with 50 wt.% PHEA and different lengths of PBLA blocks. C) APCNs with 70 wt.% PHEA and different lengths of PBLA blocks. D) WAXS data of the APCNs.

feed. Thus, PBLA00 samples correspond to the previously investigated PHEA-*l*-PDMS APCNs,^[5a,12c,44] while PBLA05 and PBLA20 correspond to the new class of peptide-reinforced PHEA-*l*-(PBLA_{*x*}-*b*-PDMS-*b*-PBLA_{*x*}) APCNs. In addition to the APCNs, samples with 0 wt.% HEA were prepared for comparison of the properties.

2.2. Secondary Structure Characterization of the APCNs

The formation of α -helices and β -sheets in the peptide-reinforced APCNs was investigated by ATR-FTIR spectroscopy (Figure 2A–C; Figure S1, Supporting Information), as spectral peaks between 1600 and 1700 cm^{-1} reveal the secondary structure of peptide segments in peptide-polymer hybrid materials. The amide I bands between 1650 and 1660 cm^{-1} can be assigned to α -helices and between 1620 and 1645 cm^{-1} to β -sheets.^[45,46] The IR spectra of PBLA00 samples (Figure 2A–C, green) do not show any peaks in this range as expected for materials not containing peptides. The spectra of peptide-containing samples (the PBLA05 and PBLA20 series) feature the amide I bands. For PBLA05, the peak corresponding to β -sheets is predominant, while for PBLA20, the spectra reveal a mix of α -helices and β -sheets. The PBLA20_70 contained 69% of β -sheets and 31% of α -helices while the PBLA20_50 and

PBLA20_30 networks contained a 1 to 1 mixture of β -sheets and α -helices (Figure 2A–C; Table S1, Supporting Information).

Wide-angle X-ray scattering (WAXS) data was used to additionally confirm the presence of α -helices and β -sheets. Figure 2D shows two peaks at $2\theta \approx 12$ and 22 for all the PBLA00 samples, which belong to the PDMS and the PHEA phases, respectively. The intensity of the $2\theta \approx 22$ peak increases with increasing PHEA content.

β -sheets of PBLA result in WAXS peaks at $2\theta \approx 5$ ($q = 0.36 \text{ \AA}^{-1}$), and α -helices usually give rise to three peak, $2\theta \approx 6, 11$ and 12 or $q = 0.45, 0.79$, and 0.9 \AA^{-1} .^[40c,47] In the peptide-containing PDMS networks, a sharp peak for PBLA05_00 at $2\theta = 5$ shows the presence of β -sheets only while the other peaks in the WAXS pattern corresponds to the PDMS phase, as deduced from a comparison with the patterns of the PDMS networks PBLA00.

For the PBLA20_00 we observe a sharp peak at $2\theta \approx 7$, which corresponds to α -helices, and less pronounced peaks arising from the PDMS, most likely because they overlap with the further peaks of the α -helical peptides. The $2\theta \approx 6$ peak has a shoulder at lower 2θ , indicating the presence of β -sheets in addition to the α -helices.

The peptide signals of the peptide-reinforced APCNs became less pronounced with increasing PHEA content, as the peptide content in the networks decreased. Nevertheless, the WAXS

patterns of all PBLA05 APCNs show the peak for presence of β -sheets, while the patterns of the PBLA20 series indicate a mixture of β -sheets and α -helices. Thus, the WAXS data supports and confirms the results from IR spectroscopy.

2.3. Morphological Characterization

As the APCNs are composed of strongly incompatible polymer chain segments, phase separation was anticipated. However, all prepared APCNs are transparent, indicating that no macroscopic phase separation occurred (Figure S2, Supporting Information). Thus, the phase separation must have occurred on the nanoscale. Small-angle X-ray scattering (SAXS) is a useful tool to characterize the nanophase morphology of APCNs as it provides the d -spacing, i.e., the average distance of the scattering phases.^[44,48] SAXS measurements of the APCNs (Figure 3A) allow determination of the d -spacing from the main peak position (q^*), as well as the radius of gyration (R_g). The latter was obtained by fitting the data to a hard-sphere interaction model, which corresponds to the pair-distance distribution function (PDDF). The d -spacing and R_g of the peptidic APCNs was higher than of the corresponding non-peptidic APCNs (Figure 3B). For example, the d -spacing of PBLA05_30 was 18.7 nm and the R_g was 3.7 nm, compared to a d -spacing of 12.8 nm and R_g of 2.7 nm of PBLA00_30. A higher PHEA content of the APCNs led to bigger d -spacing and larger R_g (Figure 3B). In the PBLA05 series, PBLA05_70 had the largest domains with a size of 21.8 nm, while in the PBLA20 series, PBLA20_70 had a d -spacing of 26.8 nm. In comparison, the non-amphiphilic networks PBLA05_00 and PBLA20_00 contained domains with sizes of 10 nm. Based on these results and the results of the measurements of mechanical properties in the following sections, it can be concluded that larger domains result in higher elasticity of the material and a larger strain-at-break.

Atomic force microscopy (AFM) was used to visualize the phase morphology of APCNs and to complement SAXS analysis. Phase mode AFM images of the surface (Figure 3D–F) and of cross-sections (Figure 3G–I) of the APCNs show phase-separated morphologies. In such images of APCNs, PDMS domains are dark and PHEA domains appear bright.^[1e,7a,13,44] The AFM images of PBLA00_50 show the typical phase morphology of PHEA-*l*-PDMS conetworks, which are interconnected, round PDMS domains in a sponge-like PHEA matrix. An accumulation of the PHEA on the surface is also observed, consistent with previous reports.^[12c,44] On the surface of the peptide-containing APCNs, domains formed on the micrometer-scale, suggesting accumulation of PDMS during free radical polymerization, particularly in the case of PBLA20_50, from which we infer that there is an effect of the PBLA length on the phase demixing of the APCNs. However, in the bulk of the APCNs, the domain size is much smaller (e.g., 19 and 18 nm thickness of the PDMS domains in PBLA05_50 and PBLA20_50, respectively) and correlates with the trend in d -spacing of the SAXS analysis (i.e., that the domains for PBLA05_50 are larger). For the PBLA05_50 APCNs, an interconnected PHEA phase with (partially) interconnected PDMS islands is observed, whereas the PBLA20_50 samples show an interconnected PDMS domain in a PHEA sponge.

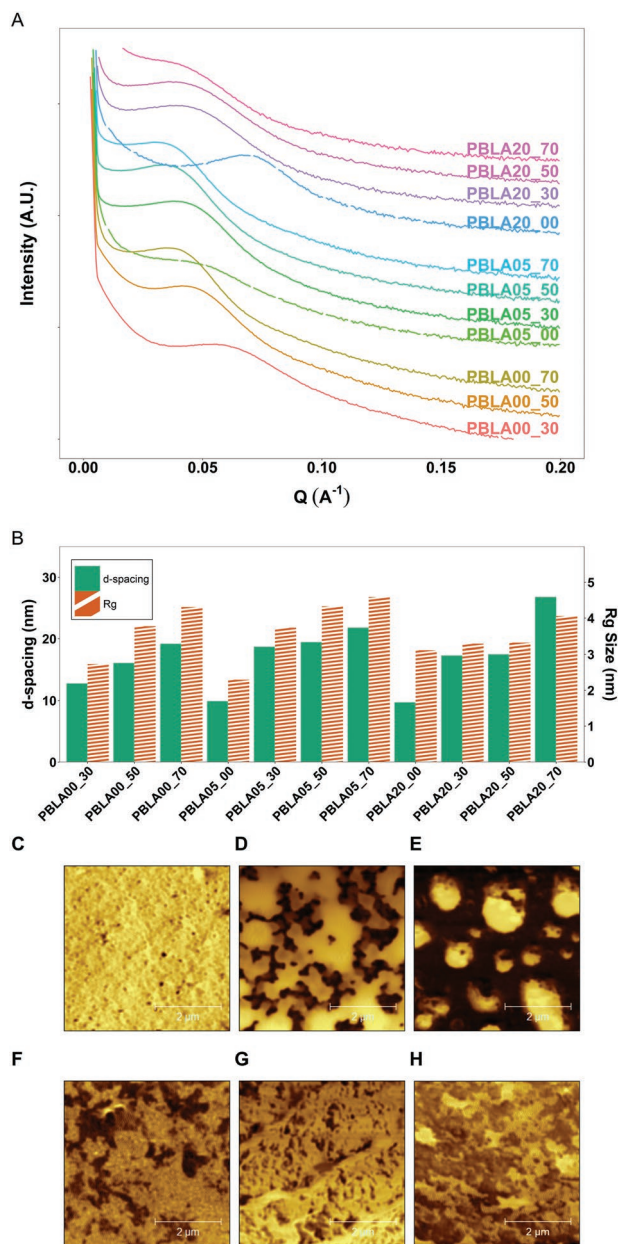


Figure 3. Characterization of the morphology of dry PHEA-*l*-(PBLA_x-*b*-PDMA_x) APCNs by SAXS and AFM. A) SAXS profiles of peptide-reinforced APCNs. B) SAXS-derived domain–domain correlation d -spacing (green) and domain sizes R_g (striped orange) of the APCNs. C–E) AFM phase mode images of APCN surfaces: C) PBLA00_50, D) PBLA05_50, E) PBLA20_50. F–H) AFM phase mode images of APCN cross-sections: F) PBLA00_50, G) PBLA05_50, H) PBLA20_50. AFM images are 5 $\mu\text{m} \times 5 \mu\text{m}$ with 2 μm scale bar.

2.4. Thermal Analysis

Because of their phase-separated morphology, APCNs typically have two glass transition temperatures (T_g^s), corresponding to the hydrophobic and hydrophilic phase, which is consistent with bicomponent polymeric systems.^[12c] The T_g of PDMS and PHEA homopolymers are -125 and -15 $^\circ\text{C}$, respectively.^[12c,49] The very low T_g of the PDMS phase could not be measured due

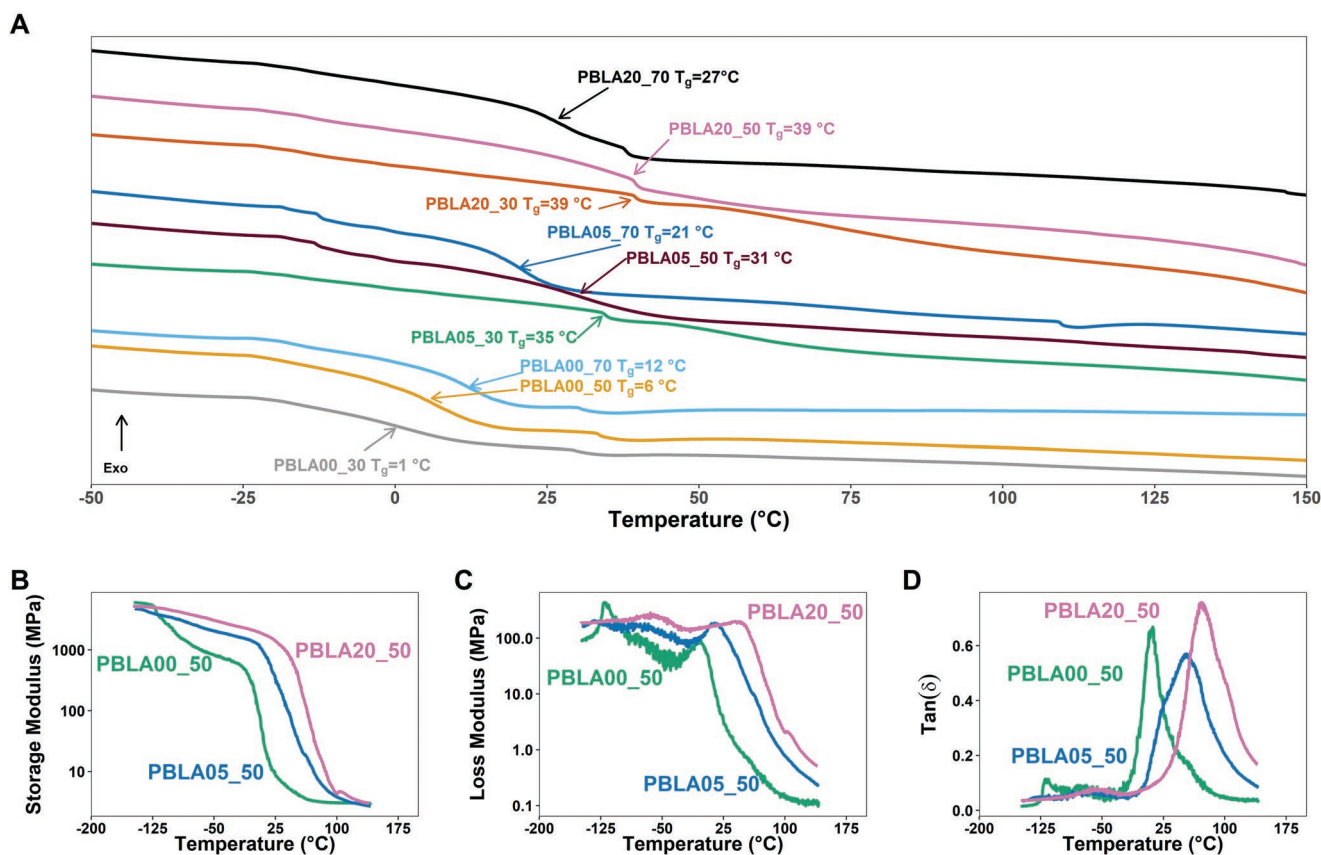


Figure 4. Characterization of the thermal properties of PHEA-*l*-PDMS and PHEA-*l*-(PBLA_{*x*}-*b*-PDMS-*b*-PBLA_{*x*}) APCNs by DSC and DMA. A) DSC curves of the different samples, with the arrows indicating the glass transition temperature of each sample. B,C) DMA temperature sweep of PBLA00_50, PBLA05_50 and PBLA20_50 samples. B) Storage modulus, C) Loss modulus, and D) Loss factor $\tan \delta$.

to instrument limitations of the scanning calorimeter used. Differential scanning calorimetry (DSC) revealed a T_g between -1 and 40°C for all APCN samples, corresponding to the hydrophilic PHEA phase and the PBLA (Figure 4A). The glass transition temperatures of APCNs with 50 wt.% HEA were 6, 31, and 39°C for the PBLA00_50, PBLA05_50, and PBLA20_50, respectively. These transitions are higher than the T_g of pure PHEA, indicating that the peptides as well as the methacrylate-based crosslinks contribute to the thermal properties of the PHEA phase. Most likely the PBLA segments are miscible with PHEA. PBLA peptides have a $T_g \approx 44^\circ\text{C}$,^[40f,47a,50] which is directly related to the PBLA20 samples, which have the highest peptide content and longer peptide chains. The PBLA20 have a higher T_g than the PBLA05 and PBLA00 samples. A higher content of PHEA increased the T_g for the non-peptidic APCNs while it decreased it for the peptidic APCNs. From this thermal response and from the AFM images (Figure 3), we observe a difference in the phase demixing between the non-peptidic and peptidic samples, inducing a shift in the T_g .

Dynamic mechanical analysis (DMA) was used to augment the DSC measurements and to measure the stiffness (storage modulus), viscous properties (loss modulus) and molecular motion (loss factor $\tan \delta$) of selected APCNs (Figure 4). For the non-peptidic network (PBLA00_50), the storage modulus (Figure 4B) drops twice (centered ≈ -111 and $\approx 7^\circ\text{C}$), which is indicative of the two glass transition temperatures. In contrast,

DMA of the peptide-containing 50 wt.% PHEA APCNs reveal only one glass transition temperature that depends on the number of peptidic repeating units. Below 0°C , the peptidic APCNs retain a higher plateau modulus than the non-peptidic APCN, implying an increased hydrogen bonding (or the formation of additional physical-crosslinks) in the APCNs. The storage modulus of the peptidic samples starts to markedly decrease above $\approx 0^\circ\text{C}$ with the midpoint of the transition indicating a T_g of 10°C for PBLA05_50 and of 45°C for PBLA20_50. The 70 wt.% PHEA samples show a similar behavior (Figure S3, Supporting Information) where a PDMS T_g could not be detected with DMA for the peptidic samples. These APCNs have a broad glass transition temperature centered at -4 and 14°C for PBLA05_70 and PBLA20_70, respectively, which is lower than the T_g of the corresponding 50 wt.% PHEA APCNs. The absence of a glass transition temperature corresponding to PDMS in the peptidic APCNs is somewhat puzzling, as the SAXS and AFM data unambiguously show two phases, proving the existence of a PDMS phase. Possibly, there are soft and hard domains, but the nature of the phase mixture creates poorly defined transitions in the storage modulus measurements, most likely due to the inhibition of the mobility of the PDMS chain segments in DMA due to the adjacent peptidic regions. This trend was also observed in other peptide reinforced materials, such as polyurethanes and polyureas.^[45,51]

The loss modulus (Figure 4C) yields information on the viscoelastic behavior. There are two peaks in all samples, corresponding to the soft domain at low temperatures and, the hard domain at higher temperatures. Thus, the loss modulus peaks verify the existence of two separated phases in the peptidic and the non-peptidic conetworks.

The loss factor $\tan \delta$ shown in Figure 4D reveals changes in the chain mobility resulting from the incorporation of peptides into the APCNs. The PBLA00_50 sample shows two $\tan \delta$ peaks, a small one at ≈ -125 °C corresponding to PDMS and a higher one at ≈ 5 °C that corresponds to PHEA. The incorporation of PBLA into the APCNs suppresses the T_g of PDMS, which is indicative of decreased PDMS mobility. This restricted molecular mobility is likely due to a morphological shift from interconnected morphology at thnano-scale to secondary structure/peptide-driven phase-separated morphology where one phase is discontinuous and the other phase is continuous (as shown in AFM phase images). This effect was also observed when increasing the hard segment content for peptidic-polyurea hybrids and hierarchical polyurethane/ureas.^[40c,45] The $\tan \delta$ peak of PBLA05 and PBLA20 shifted to higher temperatures compared to the non-peptidic APCN, which is associated with a shift in the T_g of the PHEA phase. The PBLA20 exhibits a higher T_g compared to the PBLA05, resulting in a stiffer material at room temperature. Furthermore, the $\tan \delta$ peak of PBLA05 is broader than that of PBLA20, suggesting that the PBLA05 exhibits a more heterogeneous network architecture, due to the physical crosslinks of the β -sheets.

2.5. Swelling Behavior

Due to their amphiphilic character and because they are cross-linked polymer networks, APCNs usually swell in aqueous and organic solvents. To elucidate the influence of the peptides on the swelling of the APCNs, the samples were incubated at room temperature in water and in *n*-hexane, respectively, and their volumetric degree of swelling (S_{vol}) was measured. As expected from previous work, non-peptidic PBLA00 swelled in both water and hexane. Higher PHEA content increased hydrophilic, but

decreased hydrophobic swellability (Figure 5A,B). The swelling of the peptide-reinforced APCNs in water followed the same trend, i.e., it increased with increasing PHEA content. In the composition range investigated, swelling was greatest for the 70 wt.% PHEA APCNs, reaching a S_{vol} of 1.70 ± 0.07 , 2.1 ± 0.4 , and 2.3 ± 0.4 for PBLA00_70, PBLA05_70, and PBLA20_70, respectively (Figure 5A). In other words, despite the presence of the hydrophobic PDMS and the hydrophobic PBLA segments, the APCNs swell in water. Interestingly, peptidic APCNs swell more than non-peptidic APCNs. Despite the triblock copolymer being considered hydrophobic, the PBLA repeating units can form H-bonds and induce hydrophilicity in the APCNs.

Swelling of the peptide-reinforced APCNs in organic solvents is governed by the hydrophilic-to-hydrophobic ratio of the networks and by the length of the peptide blocks (Figure 5B). For the PBLA05 series, the degree of swelling in *n*-hexane of PBLA05_30 was 1.10 ± 0.05 and decreased with increasing PHEA content because the hydrophilic-to-hydrophobic ratio of the APCNs increased. In contrast to the PBLA05 samples, the PBLA20_30, PBLA20_50, and PBLA20_70 hardly swelled at all in the nonpolar solvent, indicating that the long peptide blocks inhibited the swelling of the hydrophobic phase. This behavior is interesting, as the peptides are themselves hydrophobic. However, *n*-hexane is not able to disrupt the hydrogen bonds that hold the β -sheets and α -helices together, thus the peptide may act as a stiff scaffold, preventing the PDMS phase from expanding due to solvent uptake.

2.6. Characterization of Mechanical Properties of Peptide-Reinforced APCNs

2.6.1. Effect of PHEA Content and PBLA Repeat Length

The effect of the composition of the APCNs on their mechanical properties was investigated, for the dry samples, with uniaxial stress–strain measurements at a strain rate of 1 mm min^{-1} at room temperature. As the samples will likely be used in room temperature applications, they were tested at this temperature, even though it is within the T_g range of the materials.

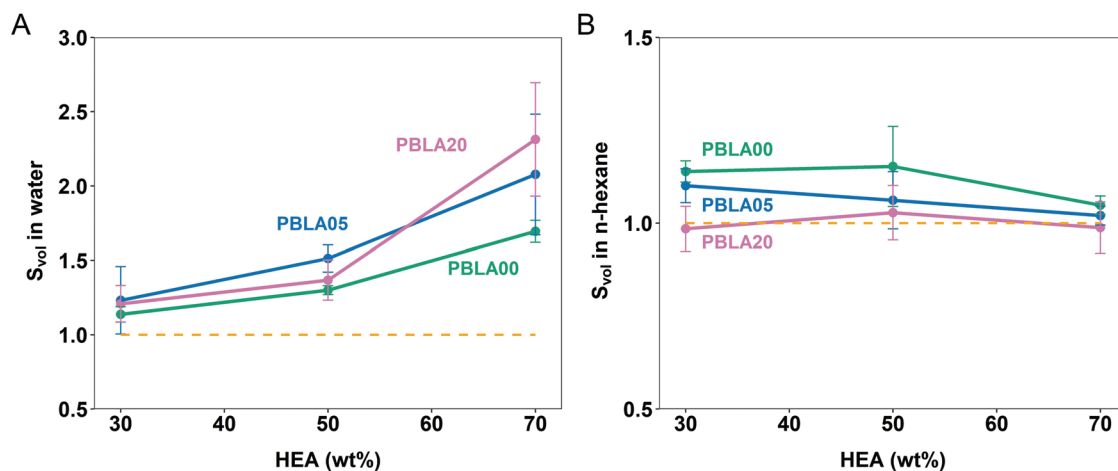


Figure 5. Swelling of APCNs as a function of the PHEA content and the peptide length. A) Volumetric degree of swelling S_{vol} in deionized water. B) Volumetric degree of swelling S_{vol} in *n*-hexane. (Mean of $n = 5$ samples \pm SD).

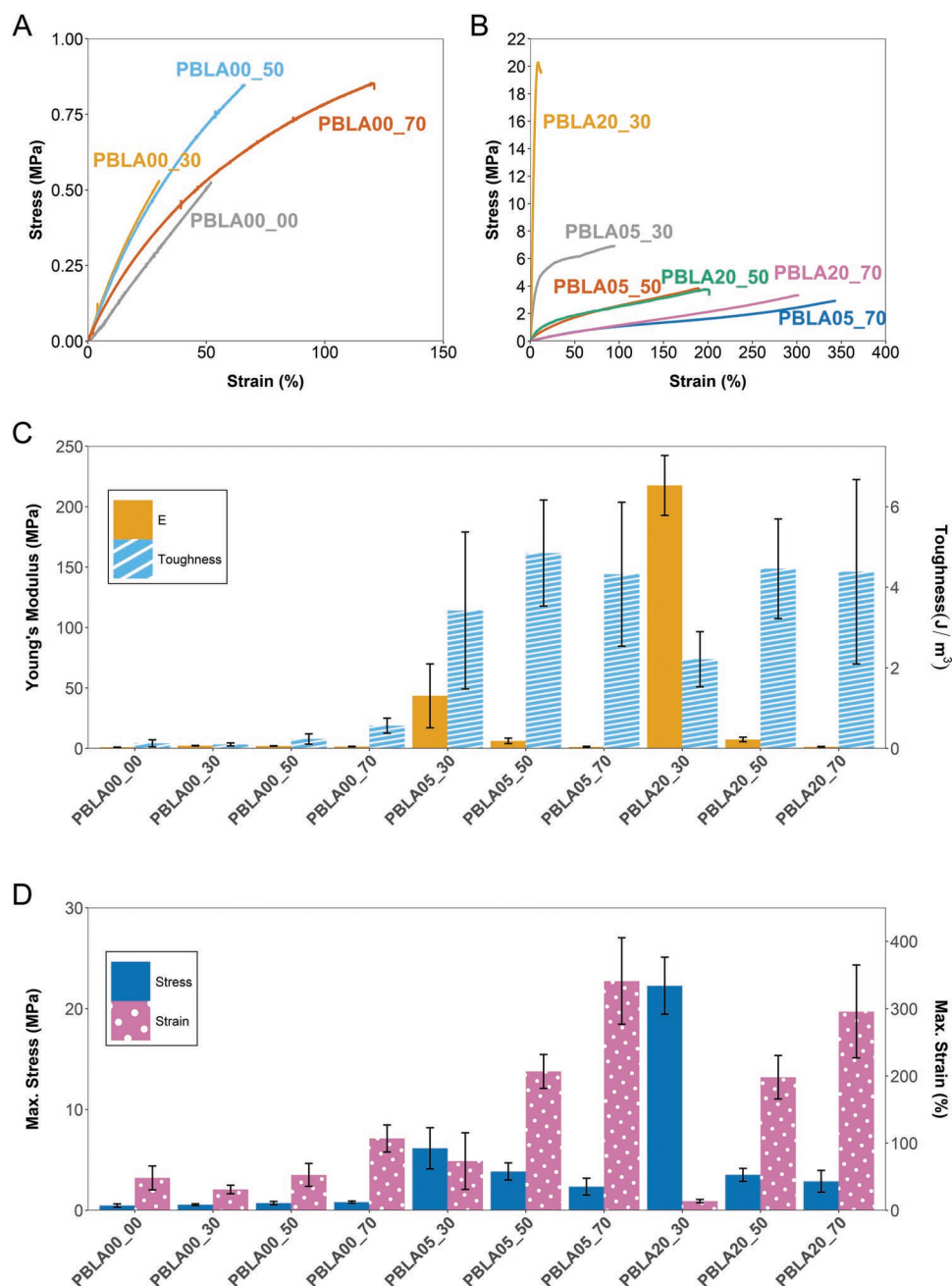


Figure 6. Mechanical data obtain from uniaxial stress–strain experiments of PHEA-*l*-PDMS and PHEA-*l*-(PBLA_{*x*}-*b*-PDMS-*b*-PBLA_{*x*}) APCNs measured at 1 mm min⁻¹. A) Stress–strain curves of PBLA00 samples with different PHEA compositions. B) Stress–strain curves of PBLA05 and PBLA20 samples with different PHEA composition. C) Summary of the Young's modulus and the toughness of the APCNs. D) Summary of the stress at break and strain at break of the APCNs. Values in panel (C) and (D) represent mean values of *n* = 8 measurements and error bars are the standard deviation.

Films of pure PDMS networks (PBLA00_00) show rubber elasticity with a Young's modulus of 1.01 ± 0.09 MPa. They can be stretched to $48 \pm 18\%$ strain before rupture, which corresponds to a toughness of 0.13 ± 0.09 MJ m⁻³ (Figure 6A–C; Figure S4, Supporting Information). Adding 30 wt.% PHEA increased the Young's modulus (*E*) to 2.25 ± 0.15 MPa while maintaining a similar toughness of 0.10 ± 0.04 MJ m⁻³ (Table S2, Supporting Information). For the PHEA-*l*-PDMS APCNs, maximum stress, strain and toughness increases and

Young's modulus decreases with increasing PHEA content (Table S2 and Figure S5, Supporting Information).

The presence of the PBLA blocks drastically altered the mechanical properties of the APCNs (Figure 6B–D). As a general trend, the materials became stiffer than their non-peptidic counterparts, and their strain-at-break as well as their toughness increased significantly. The stress–strain curves of PBLA05_30 and PBLA20_30, reveal an elastic region at low strain, followed by a yield region. The PBLA05_50, PBLA05_70,

PBLA20_50 and PBLA20_70 samples exhibit elastomeric behavior with extensibilities ranging from 190% to 340% depending upon composition.

PBLA05_30 had a Young's modulus of 43 ± 26 MPa, a strain-at-break of $73 \pm 42\%$ and a toughness of 3 ± 2 MJ m⁻³. Compared to PBLA00_30, the peptides increased the Young's modulus 100-fold. PBLA20_30 displayed an even higher Young's modulus of 218 ± 25 MPa, but the increase of the stiffness led to embrittlement and, as a result, failure at low strains. The differences in mechanical properties of the PBLA05_30 and PBLA20_30 samples can be explained by the higher fraction of β -sheets, and therefore intermolecular hydrogen bonding, in PBLA05_30. For the APCNs with a PHEA content of 50 and 70 wt.%, the mechanical properties of APCNs reinforced with different lengths of peptide blocks were similar, indicating that the morphology and overall composition had a larger influence on the mechanical properties than the difference in β -sheet content of the PBLA segments.

The fraction of the hydrophilic phase strongly influenced the properties of the peptide-reinforced APCNs. Increasing the PHEA content of the materials decreased the stress-at-break and Young's modulus, and increased strain-at-break, most likely because the effective concentration of the peptides in the materials decreased. The decrease in the stress-at-break and increase in the strain-at-break resulted in similar toughness of the 50 and 70 wt.% PHEA peptidic APCNs, which is up to 20-fold higher than the toughness of non-peptidic APCNs of the same composition. These results clearly show that the peptides reinforce the APCNs and that the mechanical properties of the materials can be tuned by the hydrophilic to hydrophobic composition, as well as the length of the peptide segments for APCNs with low PHEA content. Most likely, the reinforcement stems from the intermolecular hydrogen bonding of the β -sheets and α -helices as well as the morphology of the materials.

In the following sections, only samples with 50 and 70 wt.% PHEA are further investigated as the peptide-reinforced APCNs with a PHEA content of 30 wt.% were stiff materials that did not display the typical elasticity of APCNs that is useful for their applications.

2.6.2. Influence of Strain Rate

The mechanical properties of polymers often vary with external factors such as the strain rate that in some cases, such as spider silk, hair and polytetrafluoroethylene (PTFE), can modulate the mechanical behavior from a rubbery to a ductile or brittle material, based on the rearrangement of its internal structure.^[52] Thus, non-peptidic and peptide-reinforced APCNs were uniaxially deformed at higher strain rates (up to 500 mm min⁻¹) than in the previous section. There is little to no strain rate dependency of the mechanical properties in the PBLA00_00 and PBLA00_50 samples, i.e., in the pure PDMS network and a non-peptidic APCN (Figure 7A,B; Table S3, Figures S6, and S7, Supporting Information). The strain–stress curves at 500 mm min⁻¹ show substantial noise due to the high pulling speed (Figure 7A,B; Figure S6I,J, Supporting Information).

In contrast to the non-peptidic networks, the PBLA-reinforced APCNs show significant strain rate hardening that

increased with the strain rate, as well as toughening at higher strain rates (Figure 7). The largest strain rate-dependent hardening was observed for the PBLA05_50 samples. The Young's modulus increases from 5.8 ± 2.3 to 22.3 ± 6.3 MPa, the stress-at-break changes from 3.4 ± 0.7 to 9.8 ± 1.3 MPa, and the toughness increases from 4.1 ± 0.9 to 14 ± 4 MJ m⁻³ when comparing results from uniaxial tensile tests conducted at strain rates of 1 and 500 mm min⁻¹, respectively. For the PBLA05_70 and PBLA20_70 APCNs, a similar strain rate hardening effect was observed (Figures S8,S9 and Table S4, Supporting Information). Slow testing speeds provide sufficient time during deformation for spatial rearrangement of the PBLA segments without changes to their secondary structure. At higher strain rates, the α -helices might rearrange their structure to β -sheets thereby stiffening the APCN, similar to what has been observed for natural protein-based materials such as hair.^[52c,f]

2.6.3. Cyclic Tensile Tests

The hysteresis behavior of peptide-reinforced polymers in loading and unloading cycles of stress–strain experiments is dictated by the cleavage and reformation of physical interactions between peptide blocks, resulting in viscoelastic behavior of the materials that enhances the mechanical properties.^[40d,53] This phenomenon is also typical for many natural peptide-based materials, such as keratin,^[54] hair^[52c,f] and supramolecular systems.^[53] Pure PDMS is considered to be a soft, elastic, but low-toughness material, therefore showing no energy dissipation upon deformation, i.e., no hysteresis behavior.^[55] To analyze the hysteresis of the APCNs, three types of cyclic tensile tests were carried out, namely cyclic tests to 40% strain, cyclic tests with increasing strain in the elastic deformation range of the samples, and cyclic tests with increasing strain in the plastic deformation range of the materials (Figure 8).

Conventional non-peptidic APCNs (PBLA00_50) are elastic and exhibit only low hysteresis in all three types of measurements. In contrast, the peptide-reinforced APCNs show significant hysteresis loops, indicating that the peptides rearrange during the measurements and absorb energy, which also explains the higher toughness of the peptidic APCNs. After the first loading-unloading cycle, the cyclic test at 40% strain (Figure 8A,D; Figures S10 and S13, Supporting Information) shows similar hysteresis and maximum stress for each of the materials in each loading-unloading cycle. However, the hysteresis increases with the number of peptide repeating units from $61 \pm 2\%$ for PBLA05_50 to $82 \pm 5\%$ for PBLA20_50 at the first cycle. An explanation is that the α -helices in the latter APCN might rearrange to β -sheets when stretched, thereby absorbing additional energy, similarly to natural protein-based materials.^[52c,f] Moreover, the morphology varies with the composition. As peptides length increases, it provides additional reinforcement, through the secondary structure, balancing the inter- and intramolecular interactions. The second type of cyclic tensile experiment involves stretching the samples in their elastic regime, while increasing the strain by a certain interval in each cycle, i.e., from 5% to 80% (Figure 7B,E; Figures S11 and S14, Supporting Information). The PBLA05_50 and PBLA20_50 samples show only partial shape recovery in

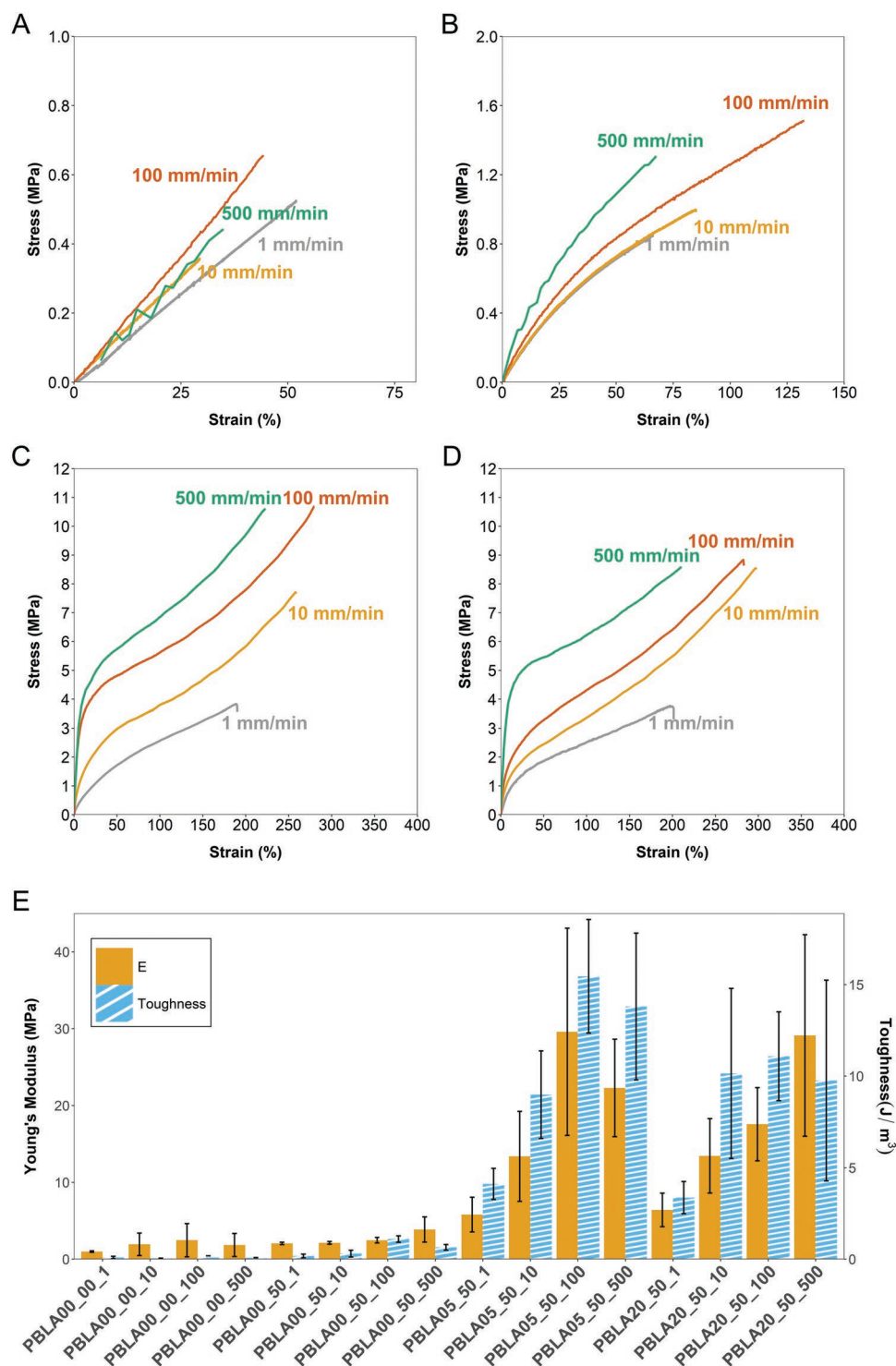


Figure 7. Strain-rate dependent uniaxial tensile tests of PHEA-*l*-PDMS and PHEA-*l*-(PBLA_{*x*}-*b*-PDMS-*b*-PBLA_{*x*}) APCNs conducted at strain rates between 1 and 500 mm min⁻¹. A) Representative stress–strain curves for PBLA00_00 samples, B) Representative stress–strain curves for PBLA00_50 samples, C) Representative stress–strain curves for PBLA05_50 samples, D) Representative stress–strain curves for PBLA20_50 samples. E) Summary of Young's modulus and toughness for the different APCN compositions at different strain rates. Samples are named PBLA_{XX}_YY_ZZZZ where XX is the number of peptide repeating units, YY is the PHEA content (wt.%) units and ZZZZ the testing speed in mm min⁻¹. Values represent mean values of *n* = 6 measurements; error bars are the standard deviation.

the elastic region, as indicated by the shift of the stress–strain curves toward higher strain in each cycle. In contrast, the

PBLA05_70 and PBLA05_70 display full recovery throughout each elastic cycle, i.e., the samples returned to their original

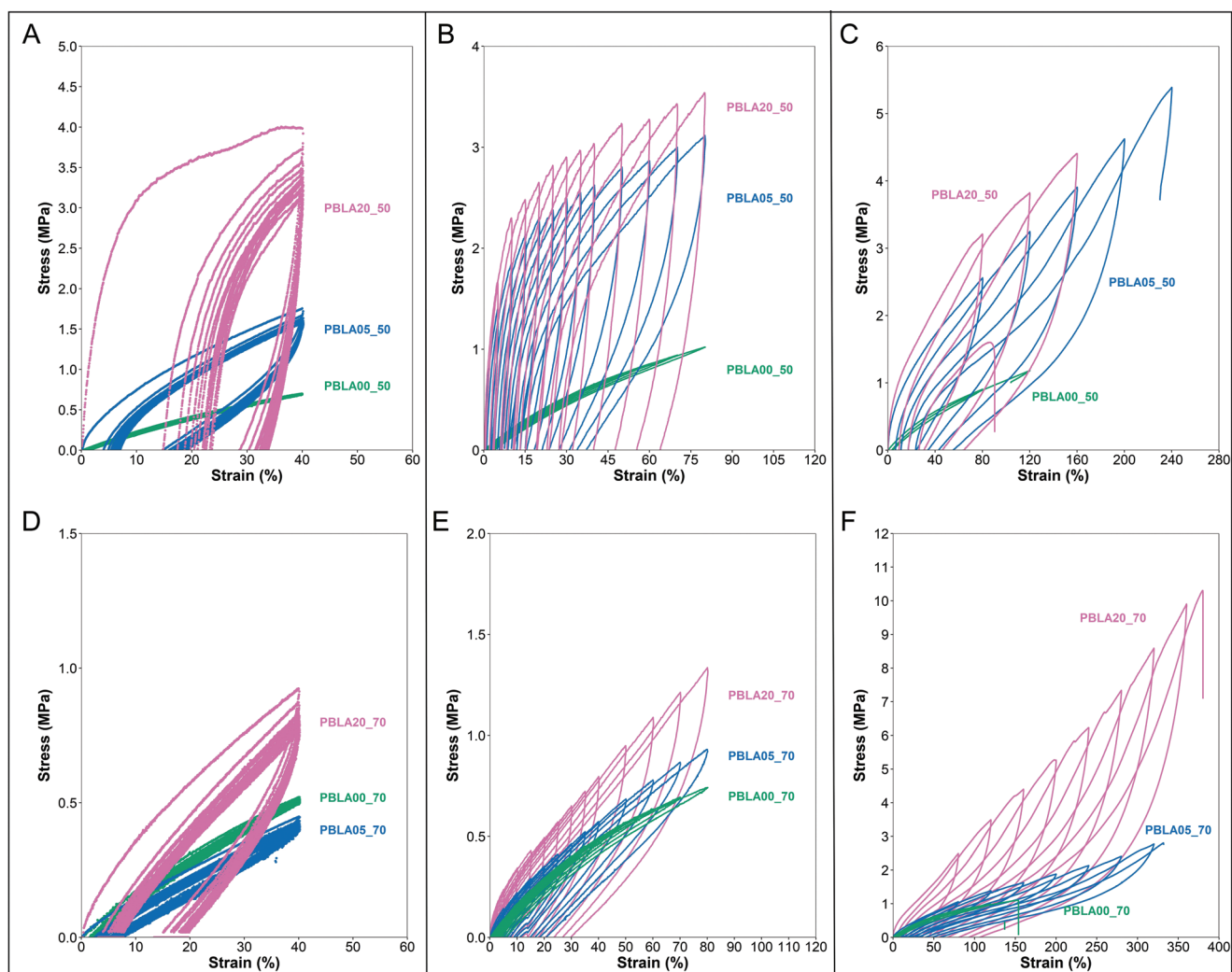


Figure 8. Cyclic tensile tests of PHEA-*l*-PDMS and PHEA-*l*-(PBLA_x-*b*-PDMS-*b*-PBLA_x) APCNs with 50 and 70 wt.% PHEA. A,D) Cyclic tests to 40% strain in each cycle. B,E) Cyclic tests in the elastic deformation range with increasing strain per cycle. C,F) Cyclic tests in the plastic deformation range with increasing strain per cycle.

dimensions when not strained, as indicated by the stress–strain curves starting from the origin of the graph. Most likely, the elastic properties of the PHEA chains in the 70% PHEA APCN dominate shape recovery compared to the 50% PHEA APCNs, which have a larger influence of the peptidic units. Interestingly, the length of the PBLA block, and therefore the predominance of β -sheets or α -helices, does not impact this difference in the elastic recovery of the APCNs.

The third type of cyclic test elongates the samples into their plastic deformation range, while increasing the strain in each cycle, i.e., starting from 80% strain and then increasing the strain by 40% in each cycle (Figure 7C,F; Figures S12 and S15, Supporting Information). Again, PBLA05_50 and PBLA20_50 only partially recover their shape at the end of each cycle. PBLA05_70 and PBLA00_70 also show non-recovered deformation after each tensile cycle, but this effect is less pronounced than for the 50 wt.% PHEA samples. Thus, when stretched into their plastic deformation range, all investigated peptide-reinforced APCNs deformed plastically, which is a further proof

of their viscoelastic behavior induced by the presence of PBLA blocks.

2.6.4. Solvent-Induced Recovery of the Shape of Deformed APCNs

The residual deformation after uniaxial tensile tests of the peptide-reinforced APCNs is due to non-recovered deformation of the PBLA blocks. However, APCNs have the ability to swell in both hydrocarbons and water. The elastic properties of the underlying PHEA-*l*-PDMS APCNs may allow the peptides to recover their original structure when the networks are swollen, thereby recovering the original shape of the material after drying.

The shape recovery was analyzed by measuring the length of PBLA05_50 samples before mechanical deformation, after they had been stretched to 100% strain and relaxed, and after the deformed APCNs had been swollen in *n*-hexane for 20 min and dried under vacuum at 60 °C. This cycle was carried out

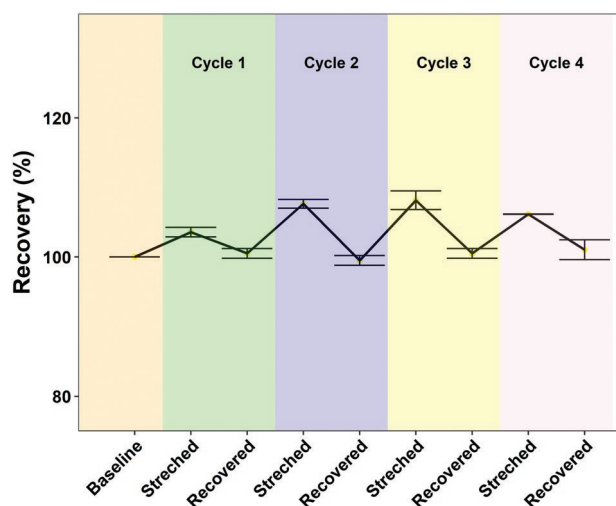


Figure 9. Shape deformation and recovery of PBLA05_50 upon plastic deformation and subsequent swelling in *n*-hexane and drying. The length of an APCN sample was measured before deformation (baseline) and set to 100%. Then, the sample was deformed to 100% strain and relaxed (stretched), treated with solvent and dried again (recovered). The sample was immersed in *n*-hexane for 20 min and dried in vacuum, and the deformation-recovery cycle repeated. Values represent mean values of $n = 3$ samples; error bars are the standard deviation.

multiple times. The peptidic APCNs maintain a similar maximum strain and stress during each cycle (Figure S16, Supporting Information) and fully recover their original size after the solvent treatment in each cycle (Figure 9). Thus, the shape and the mechanical properties of the peptide-reinforced APCNs can be fully recovered after a plastic deformation event by simple swelling and drying, which indicates that the force-dissipating peptidic structures in the APCNs can be regenerated. Moreover, this property could become very useful to extend the service life time of these APCNs in their applications and hints toward possible shape-memory applications of such APCNs.

3. Conclusion

The possibility of tailoring and enhancing the mechanical properties of APCNs by using peptide-bearing PDMS crosslinkers instead of conventional PDMS crosslinkers was demonstrated. The PBLA blocks enabled stiffer, stronger, and tougher conetworks (Figure 10) while their elastic properties, transparency, characteristic swellability in water and, for the PBLA_05 networks, swellability in solvents of opposing polarity were retained. The incorporation of peptides into the APCNs increased the maximum stress that the materials can withstand up to 40-fold and increased the maximum strain to up to 340%, with a higher toughness of up to $4.85 \pm 1.32 \text{ MJ m}^{-3}$. The length of the peptide blocks influenced the physical and mechanical properties of the APCNs, which could therefore be tailored to specific applications. The stress-strain curves that were recorded at different strain rates show strain hardening of the peptidic APCNs. Moreover, peptide-reinforced APCNs show substantial hysteresis in stress-strain experiments, indicating that the peptidic structures in the materials rearrange and

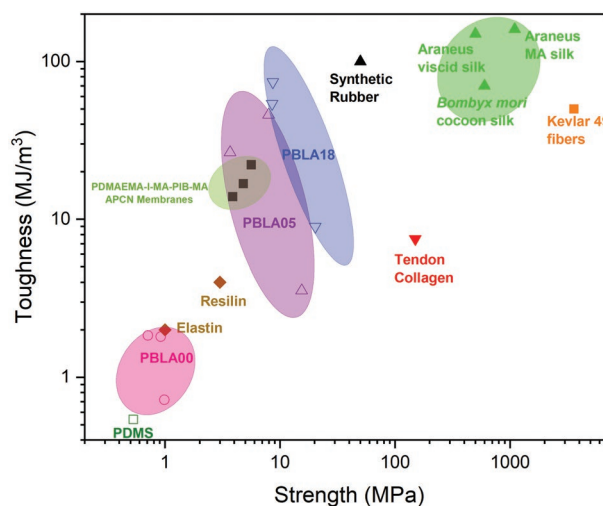


Figure 10. Ashby plot comparing the key mechanical properties of the peptide-reinforced PHEA-*l*-(PBLA_{*x*}-*b*-PDMS-*b*-PBLA_{*x*}) APCNs with conventional PDMS-based APCNs, PIB-based APCNs, as well as natural materials such as spider silk, resilin, elastin, and tendon collagen. Data for the Ashby plot taken from references.^[15a,b,56]

thereby dissipate energy, a mechanism that contributes to their high toughness. Even when “permanently” deformed in tensile tests, simple swelling in hexane followed by drying allowed the original shape of APCNs to be recovered.

Finally, free radical copolymerization of TMS-HEA with α,ω -dimethacrylate functionalized peptide-PDMS-peptide triblock copolymer crosslinkers, followed by cleavage of the TMS groups, is a straight forward method to produce APCNs with significantly enhanced mechanical properties that outperform conventional PHEA-*l*-PDMS APCNs and, in the case of PBLA20-based conetworks, also APCNs based on polyisobutylene (PIB)^[56] that already have higher mechanical properties than PHEA-*l*-PDMS conetworks (Figure 10). Compared to some natural materials, the peptide-reinforced APCNs have higher strength and toughness than elastin and resilin, but have not reached the mechanical properties of nature’s most sophisticated structural proteins such as silks (Figure 10). The bio-inspired strategy to reinforce APCNs with peptides is likely to be readily transferable to other APCNs, e.g. those based on PIB crosslinkers,^[56,57] and to other type of polymer networks such as hydrogels and lyogels. Given the wide range of applications of APCNs in general and PHEA-*l*-PDMS conetworks in particular, peptide-reinforced APCN might greatly widen the applicability of these materials in scenarios where aqueous swelling of the polymer networks and excellent mechanical properties are important, such as extended wear soft contact lenses, biomaterials, membranes, and catalytic materials.

4. Experimental Section

Materials: Commercial α,ω -methacryloxypropyl-terminated poly(dimethylsiloxane) (MA-PDMS-MA, viscosity 50–90 cSt, molecular weight = 4500–5500 g mol^{-1}) was purchased from ABCR (Germany). Bis(3-aminopropyl) terminated polydimethylsiloxane (PDMS, molecular weight = 2500 g mol^{-1}), β -benzyl-L-aspartate (BLA), triphosgene, isocynoethyl methacrylate, dibutyltin dilaurate, 2-hydroxyethyl

acrylate, triethylamine, chlorotrimethylsilane, photoinitiator bis(2,4,6-trimethylbenzoyl)-phenylphosphineoxide (Irgacure 819) and all analytical grade solvents were purchased from Sigma–Aldrich and used as received except for PDMS. Adhesive polypropylene tape (50 μm thickness) was bought from Tesa, Germany.

Synthesis of TMS-HEA: The TMS-HEA was prepared based on previous literature procedures.^[58]

Synthesis of PBLA_x-b-PDMS-b-PBLA_x Triblock Copolymers and Functionalization of the Chain Ends with MA End Groups: The PBLA_x-b-PDMS-b-PBLA_x triblock copolymers were synthesized through amine-initiated *N*-carboxyanhydride (NCA) polymerization via ring opening of β-benzyl-L-aspartic acid *N*-carboxyanhydride (synthesized via established literature procedures)^[59] from α,ω-amine-terminated PDMS as previously described.^[40f,45,60] The molar ratios (monomer/initiator) were chosen according to the desired peptidic block lengths, *x* = 5 and 20 repeating units. PBLA repeat length of the final material was measured by NMR spectroscopy (Figure S17, Supporting Information). The PBLA₅-b-PDMS-b-PBLA₅ and PBLA₂₀-b-PDMS-b-PBLA₂₀ triblock copolymers had an overall number-average molecular weight (*M_n*) of 11 700 and 3700 g mol⁻¹, and a PDMS:PBLA weight ratio of 1.53 and 0.38, respectively, which was determined by gel permeation chromatography (GPC) (Figure S18, Supporting Information) and proton nuclear magnetic resonance (¹H NMR) spectroscopy. Synthetic yields were ≈75 and 70%, respectively.

The chain ends of PBLA_x-PDMS- PBLA_x were modified with methacrylate (MA) groups by reaction with isocynoethyl methacrylate. The triblock copolymer (2.0 g) was mixed with of THF (40 mL) as solvent and 0.4 mL of isocynoethyl methacrylate (439 mg, 2.83 mmol). Tin dibutyl dilaurate (552 μL, 580 mg, 631.56 mmol) was added dropwise. The reaction was left stirring at room temperature overnight. The solvent was evaporated using a rotary evaporator, the samples were purified by extraction with cold *n*-hexane and THF, and the resulting product placed in a vacuum oven to dry overnight at 50 °C and 100 mbar. The NMR is presented in Figure S19 (Supporting Information).

Synthesis of APCNs: APCNs of different compositions (weight ratios of TMS-HEA and hydrophobic macrocrosslinkers: Table 1), were synthesized by UV-induced free radical polymerization Figure 1. For the non-peptidic APCNs, the TMS-HEA was directly vortexed with the crosslinkers using a Vortex 3 shaker (IKA) and afterward the initiator in powder form was added and the solution was mixed by vortexing. For the peptide-reinforced APCNs, the MA terminated triblock copolymer was mixed with DMSO to dissolve the solid MA-PBLA_x-b-PDMS-b-PBLA_x-MA, vortexed for 1 min, left in an ultrasonic bath (Ultrawave Q series) for 30 min at 25 °C, and vortexed again for 1 min. Afterward, the TMS-HEA was mixed into the solution under vortexing. As a final step, the initiator was added as described above. The mixture was placed onto a glass microscopy slide covered with Tesa tape. The thickness of the mold was set by a stack of four Tesa stripes, 50 μm each, at both ends of the microscopy slide, giving a final thickness of 200 μm. Afterward, the system was covered with a second glass slide covered with Tesa tape, placed in a UV flood lamp system (Dymax 500), and irradiated for 9 min from each side. Subsequently, the APCNs were removed from the Tesa tape-coated glass slides and placed, to cleave the TMS groups off the polymer and to generate the hydrophilic PHEA phase, into 200 mL of a 1:1 v:v isopropanol:H₂O solvent mixture overnight at room temperature, followed by incubation in 200 mL methanol overnight. Finally, the samples were dried in a vacuum oven at 100 mbar and 50 °C for 2 h.

Swelling of APCNs: The swelling behavior of the APCNs was measured by immersing samples of ≈ 3 mm x 6 mm in *n*-hexane and distilled water, respectively, overnight at room temperature. The edge length (*L_i*) was measured for the dry and swollen samples using an optical microscope (Leitz Ergolux reflected light). The volumetric degree of swelling, *S_{vol}*, was determined from the edges of the sample as:

$$S_{vol} = \frac{1}{n} \sum_{i=1}^n \left(\frac{L_{i,swollen}}{L_{i,dry}} \right)^3 \quad (1)$$

where *n* denotes the number of edges.

NMR Spectroscopy: ¹H NMR spectroscopy was measured using Bruker AV400 (Figure S19, Supporting Information) and 600 MHz (Figure S17, Supporting Information) spectrometers. CDCl₃ and (CD₃)₂SO were used as solvents for the triblock copolymers before and after functionalization, respectively.

GPC: Measurements were performed using a TOSOH Bioscience GPC (HLC-8420 GPC) equipped with refractive index and variable wavelength detectors. The measurements were in dimethylacetamide/LiBr (0.5 wt.%) as eluent, with a solvent flow rate of 0.4 mL min⁻¹, at 50 °C. PMMA was used as standard (8 standards: 2210, 675.5, 146.5, and 72 kDa, 30 780, 9150, 4760, and 1840 Da).

ATR-FTIR Spectroscopy of APCNs: Attenuated total reflection – Fourier transform infrared (ATR-FTIR) spectroscopy was used to analyze presence and content of β-sheets and α-helices in the peptidic-APCNs and the peptidic triblock copolymers using an Agilent 5500 A series spectrometer equipped with a diamond ATR crystal. All samples were measured in absorbance mode with 128 scans. MicroLab was used to obtain and analyze the spectra.

SAXS and WAXS: SAXS measurements were performed using a Xenocs Xeuss 2.0. For the measurements, X-rays were generated at 50 kV/0.6 Ma at a beam wavelength of 1.542 Å (Cu Kα radiation) and sample-to-detector distances of 1200 and 72 mm, respectively, for SAXS and WAXS. The scattered beam was recorded on a CCD detector with a pixel resolution of 172 × 172 μm. The scattering patterns of APCN films (≈1.5 × 1.5 cm²) were recorded over 60 min of exposure time at room temperature. 2D patterns were azimuthally integrated to obtain the scattering intensity as a function of scattering vector, *q*, where *q* = 4πsin(θ)/λ. 2θ was the scattering angle. The azimuthal integration was obtained by using the software Foxtrot 3.4.9.

Atomic Force Microscopy: Atomic force microscopy (AFM) was conducted in tapping mode with a silicon AFM probe (Tap-150Al-G, BudgetSensors, Bulgaria) with a force constant of 5 N m⁻¹ and resonance frequency of 150 kHz under ambient conditions. Measurements were performed of the sample surface and the cross-section. For the cross-section, the samples were frozen in liquid nitrogen and cut with a razor blade in order to obtain a smooth cut. The instrument used was a Bruker Innova Atomic Force Microscope. The images were analyzed using Gwyddion software (Version 2.55).

DSC: Differential scanning calorimetry (DSC) was measured using a TA Instruments Q20. All the samples were measured for two cycles at a heating and cooling rate of 10 °C min⁻¹, from –50 to 150 °C to –50 °C. The glass transition temperature was determined from the transition mid-point of the second heating curve.

DMA: Dynamic mechanical analysis (DMA) measurements were performed using a TA Instruments DMA Q800 in tensile mode. The APCNs were cut into rectangular strips of a width of 2.8 mm and a length of ≈12 mm so that the measurement length of the sample was maintained at ≈10 mm. Experiments were conducted in a range of –150 to 150 °C. A heating rate of 10 °C min⁻¹ and a strain amplitude of 10 μm at a frequency of 1 Hz was applied.

Tensile Tests: The mechanical properties were measured using a Testometric M250-2.5 CT tensile machine with a 100 N load cell. A total of eight samples (except for PBLA20_30 due to the fragility of the samples) of each type of APCN were tested at a speed of 1 mm min⁻¹. Speeds of 10, 100 and 500 mm min⁻¹ were used to test the effect of the strain rate on the mechanical properties. The samples were cut in dog bone shape following DIN 53504 S3 specifications with sample thickness of ≈0.2 mm. All tests were performed with dry samples at temperatures between 20–23 °C and humidity between 25–38%.

Cyclic Tensile Tests: The cyclic tests were performed using a Testometric M250-2.5CT. The samples were cut in dog bone shape following DIN 53504 S3 specifications with a sample thickness of ≈0.2 mm. All tests were performed, for dry samples, at temperatures between 20–23 °C and humidity between 25–38% and a speed of 10 mm min⁻¹. The 40% strain cyclic tests were performed for 15 cycles. The cyclic elastic tests were performed for strains of 5, 10, 15, 20, 25, 30, 35, 40, 50, 60, 70, and 80%. The cyclic plastic tests were performed for strains of 80, 120, 160, 200,

240, 280, 320, and 360% maximum depending on the breaking point of the sample.

Shape-Recovery Cyclic Tests: The cyclic tests were performed using a Testometric M250-2.5CT. The samples were cut in dog bone shape following DIN 53504 S3 specifications with a sample thickness of ≈ 0.2 mm. The length of the samples was measured by placing the samples on mm paper, marking the length of the whole dog bone as the clamping regions don't deform, and measuring the length using image analysis software Fiji. All tests were performed, for dry samples, at temperatures between 20–23 °C and humidity between 25–38%. The samples were stretched to a strain of 100% at a strain rate of 10 mm min⁻¹ in each cycle. The samples were removed from the tensile tester and their deformed length measured as indicated above. Afterward, the samples were placed to recover in *n*-hexane for 20 min and dried in a vacuum oven (100 mbar at 60 °C) for 20 min and left at room atmosphere for 20 min before measuring their length again. The cycles were repeated until the sample failed.

Supporting Information

Supporting Information is available from the Wiley Online Library or from the author.

Acknowledgements

The project received funding from the Partnership for International Research and Education (PIRE) Bio-inspired Materials and Systems, supported by the U.S. National Science Foundation under Grant No. OISE 1844463 and the Swiss National Science Foundation under Grant No. IZPIPO_177995. Moreover, this work benefitted from support from the Swiss National Science Foundation through the National Center of Competence in Research (NCCR) Bio-Inspired Materials (Grant No. 51NF40-182881). The authors thank Dr. Michael Stringer for assistance with data analysis and mathematical discussions.

Open access funding enabled and organized by Projekt DEAL.

Conflict of Interest

The authors declare no conflict of interest.

Data Availability Statement

The data that support the findings of this study are available from the corresponding author upon reasonable request.

Keywords

amphiphilic polymer networks, bio-inspired polymeric materials, hydrogels, mechanical properties, peptide-polymer hybrids, peptides, polymer reinforcements

Received: June 27, 2022

Revised: September 19, 2022

Published online: October 17, 2022

- [1] a) C. S. Patrickios, T. K. Georgiou, *Curr. Opin. Colloid Interface Sci.* **2003**, *8*, 76; b) G. Erdodi, J. P. Kennedy, *Prog. Polym. Sci.* **2006**, *31*, 1; c) L. Mespouille, J. L. Hedrick, P. Dubois, *Soft Matter* **2009**, *5*, 4878;

- d) C. S. Patrickios, in *Amphiphilic Polymer Co-networks: Synthesis, Properties, Modelling and Applications*, (Ed: C. S. Patrickios), The Royal Society of Chemistry, Cambridge, UK **2020**, pp. 1–14; e) S. Ulrich, L. F. Boesel, N. Bruns, in *Amphiphilic Polymer Co-networks: Synthesis, Properties, Modelling and Applications*, (Ed: C. S. Patrickios), The Royal Society of Chemistry, Cambridge, UK **2020**, pp. 331–363; f) C. S. Patrickios, K. Matyjaszewski, *Polym. Int.* **2021**, *70*, 10.
- [2] a) G. Guzman, S. S. Es-haghi, T. Nugay, M. Cakmak, *Adv. Healthcare Mater* **2017**, *6*, 1600775; b) C. Zhang, Z. Liu, H. Wang, X. Feng, C. He, *Macromol. Biosci.* **2017**, *17*, 1600444; c) Z. Mutlu, S. Shams Es-haghi, M. Cakmak, *Adv. Healthcare Mater.* **2019**, *8*, 1801390.
- [3] a) I. S. Isayeva, B. T. Kasibhatla, K. S. Rosenthal, J. P. Kennedy, *Bio-materials* **2003**, *24*, 3483; b) G. Erdodi, J. Kang, B. Yalcin, M. Cakmak, K. S. Rosenthal, S. Grundfest-Broniatowski, J. P. Kennedy, *Biomed. Microdevices* **2009**, *11*, 297; c) J. Kang, G. Erdodi, J. P. Kennedy, H. Chou, L. Lu, S. Grundfest-Broniatowski, *Macromol. Biosci.* **2010**, *10*, 369; d) G. Guzman, T. Nugay, I. Nugay, N. Nugay, J. Kennedy, M. Cakmak, *Macromolecules* **2015**, *48*, 6251.
- [4] a) A. K. S. Chandel, C. U. Kumar, S. K. Jewrajka, *ACS Appl. Mater. Interfaces* **2016**, *8*, 3182; b) B. Nutan, A. K. S. Chandel, D. V. Bhalani, S. K. Jewrajka, *Polymer* **2017**, *111*, 265.
- [5] a) N. Bruns, J. C. Tiller, *Nano Lett.* **2005**, *5*, 45; b) N. Bruns, W. Bannwarth, J. C. Tiller, *Biotechnol. Bioeng.* **2008**, *101*, 19; c) S. Dech, V. Wruk, C. P. Fik, J. C. Tiller, *Polymer* **2012**, *53*, 701; d) I. Sittko, K. Kremser, M. Roth, S. Kuehne, S. Stuhr, J. C. Tiller, *Polymer* **2015**, *64*, 122.
- [6] a) M. Hanko, N. Bruns, J. C. Tiller, J. Heinze, *Anal. Bioanal. Chem.* **2006**, *386*, 1273; b) M. Hanko, N. Bruns, S. Rentmeister, J. C. Tiller, J. Heinze, *Anal. Chem.* **2006**, *78*, 6376; c) S. Ulrich, A. Osypova, G. Panzarasa, R. M. Rossi, N. Bruns, L. F. Boesel, *Macromol. Rapid Commun.* **2019**, *40*, 1900360.
- [7] a) K. Schöller, S. Küpfer, L. Baumann, P. M. Hoyer, D. de Courten, R. M. Rossi, A. Vetushka, M. Wolf, N. Bruns, L. J. Scherer, *Adv. Funct. Mater.* **2014**, *24*, 5194; b) K. Scholler, C. Toncelli, J. Experton, S. Widmer, D. Rentsch, A. Vetushka, C. J. Martin, M. Heuberger, C. E. Housecroft, E. C. Constable, L. F. Boesel, L. J. Scherer, *RSC Adv.* **2016**, *6*, 97921.
- [8] M. Rother, J. Barmettler, A. Reichmuth, J. V. Araujo, C. Rytka, O. Glaied, U. Pieleas, N. Bruns, *Adv. Mater.* **2015**, *27*, 6620.
- [9] a) F. E. Du Prez, E. J. Goethals, R. Schue, H. Qariouh, F. Schue, *Polym. Int.* **1998**, *46*, 117; b) X. Li, M. Basko, F. Du Prez, I. F. J. Vankelecom, *J. Phys. Chem. B* **2008**, *112*, 16539; c) J. Tobis, L. Boch, Y. Thomann, J. C. Tiller, *J. Membr. Sci.* **2011**, *372*, 219.
- [10] H. Wang, C. Zhang, J. Wang, X. Feng, C. He, *ACS Sustainable Chem. Eng.* **2016**, *4*, 3803.
- [11] a) C.-S. Huang, K. Jakubowski, S. Ulrich, S. Yakunin, M. Clerc, C. Toncelli, R. M. Rossi, M. V. Kovalenko, L. F. Boesel, *Nano Energy* **2020**, *76*, 105039; b) C.-S. Huang, S. Yakunin, J. Avaro, X. Kang, M. I. Bodnarchuk, M. Liebi, X. Sun, R. M. Rossi, M. V. Kovalenko, L. F. Boesel, *Adv. Energy Mater.* **2022**, *12*, 2200441.
- [12] a) J. Scherble, R. Thomann, B. Ivan, R. Mülhaupt, *J. Polym. Sci., Part B: Polym. Phys.* **2001**, *39*, 1429; b) B. Iván, M. Haraszti, G. Erdódi, J. Scherble, R. Thomann, R. Mülhaupt, *Macromol. Symp.* **2005**, *227*, 265; c) N. Bruns, J. Scherble, L. Hartmann, R. Thomann, B. Iván, R. Mülhaupt, J. C. Tiller, *Macromolecules* **2005**, *38*, 2431; d) C. Fodor, G. Kali, R. Thomann, Y. Thomann, B. Ivan, R. Mülhaupt, *RSC Adv.* **2017**, *7*, 6827; e) T. Stumphäuser, G. Kasza, A. Domján, A. Wacha, Z. Varga, Y. Thomann, R. Thomann, B. Pásztói, T. M. Trötschler, B. Kersch, R. Mülhaupt, B. Iván, *Polymers* **2020**, *12*, 2292.
- [13] N. Bruns, J. C. Tiller, *Macromolecules* **2006**, *39*, 4386.
- [14] a) P. Calvert, *Adv. Mater.* **2009**, *21*, 743; b) S. Fuchs, K. Shariati, M. Ma, *Adv. Healthcare Mater.* **2020**, *9*, 1901396.
- [15] a) J. M. Gosline, P. A. Guerette, C. S. Ortlepp, K. N. Savage, *J Exp Biol* **1999**, *202*, 3295; b) J. C. Johnson, L. T. J. Korley, *Soft Matter*

- 2012, 8, 11431; c) J. Hua, P. F. Ng, B. Fei, *J. Polym. Sci., Part B: Polym. Phys.* **2018**, 56, 1325.
- [16] S. Tan, N. J.-A. Chan, J. Collins, Q. Fu, G. G. Qiao, in *Amphiphilic Polymer Co-networks*, (Ed: C. S. Patrickios), The Royal Society of Chemistry, Cambridge, UK **2020**, pp. 277–308.
- [17] Z. Liu, P. Calvert, *Adv. Mater.* **2000**, 12, 288.
- [18] E. Palleau, D. Morales, M. D. Dickey, O. D. Velev, *Nat. Commun.* **2013**, 4, 2257.
- [19] Y. Takishima, K. Yoshida, A. Khosla, M. Kawakami, H. Furukawa, *ECS J. Solid State Sci. Technol.* **2021**, 10, 037002.
- [20] a) Y. Xu, Z. Lin, X. Huang, Y. Liu, Y. Huang, X. Duan, *ACS Nano* **2013**, 7, 4042; b) K. Wang, X. Zhang, C. Li, H. Zhang, X. Sun, N. Xu, Y. Ma, *J. Mater. Chem. A* **2014**, 2, 19726.
- [21] S. Mantha, S. Pillai, P. Khayambashi, A. Upadhyay, Y. Zhang, O. Tao, H. M. Pham, S. D. Tran, *Materials* **2019**, 12, 3323.
- [22] S. Hume, G. Hithell, G. M. Greetham, P. M. Donaldson, M. Towrie, A. W. Parker, M. J. Baker, N. T. Hunt, *Chem. Sci.* **2019**, 10, 6448.
- [23] Z. Wang, X. Zheng, T. Ouchi, T. B. Kouznetsova, H. K. Beech, S. Av-Ron, T. Matsuda, B. H. Bowser, S. Wang, J. A. Johnson, J. A. Kalow, B. D. Olsen, J. P. Gong, M. Rubinstein, S. L. Craig, *Science* **2021**, 374, 193.
- [24] J. Kim, G. Zhang, M. Shi, Z. Suo, *Science* **2021**, 374, 212.
- [25] J.-Y. Sun, X. Zhao, W. R. K. Illeperuma, O. Chaudhuri, K. H. Oh, D. J. Mooney, J. J. Vlassak, Z. Suo, *Nature* **2012**, 489, 133.
- [26] H. Yin, D. R. King, T. L. Sun, Y. Saruwatari, T. Nakajima, T. Kurokawa, J. P. Gong, *ACS Appl. Mater. Interfaces* **2020**, 12, 50068.
- [27] M. Hua, S. Wu, Y. Ma, Y. Zhao, Z. Chen, I. Frenkel, J. Strzalka, H. Zhou, X. Zhu, X. He, *Nature* **2021**, 590, 594.
- [28] a) U. M. Krishna, A. W. Martinez, J. M. Caves, E. L. Chaikof, *Acta Biomater.* **2012**, 8, 988; b) B. Ozcelik, K. D. Brown, A. Blencowe, K. Ladewig, G. W. Stevens, J. P. Scheerlinck, K. Abberton, M. Daniell, G. G. Qiao, *Adv. Healthcare Mater.* **2014**, 3, 1496; c) K. Li, C. Zhou, S. Liu, F. Yao, G. Fu, L. Xu, *React. Funct. Polym.* **2017**, 117, 81.
- [29] a) C.-J. Wu, A. K. Gaharwar, B. K. Chan, G. Schmidt, *Macromolecules* **2011**, 44, 8215; b) C. Zhang, N. Sangaj, Y. Hwang, A. Phadke, C.-W. Chang, S. Varghese, *Acta Biomater.* **2011**, 7, 3362.
- [30] D. Gu, S. Tan, C. Xu, A. J. O'Connor, G. G. Qiao, *Chem. Commun.* **2017**, 53, 6756.
- [31] a) A. Ghoorchian, J. R. Simon, B. Bharti, W. Han, X. Zhao, A. Chilkoti, G. P. López, *Adv. Funct. Mater.* **2015**, 25, 3122; b) T. S. Anirudhan, J. Parvathy, A. S. Nair, *Carbohydr. Polym.* **2016**, 136, 1118.
- [32] a) E. J. Kepola, E. Loizou, C. S. Patrickios, E. Leontidis, C. Voutouri, T. Stylianopoulos, R. Schweins, M. Gradzielski, C. Krumm, J. C. Tiller, M. Kushnir, C. Wesdemiotis, *ACS Macro Lett.* **2015**, 4, 1163; b) E. J. Kepola, K. Kyriacou, C. S. Patrickios, M. Simon, M. Gradzielski, M. Kushnir, C. Wesdemiotis, *Macromol. Symp.* **2017**, 372, 69.
- [33] a) H. Jia, Z. Huang, Z. Fei, P. J. Dyson, Z. Zheng, X. Wang, *ACS Appl. Mater. Interfaces* **2016**, 8, 31339; b) H. J. Zhang, T. L. Sun, A. K. Zhang, Y. Ikura, T. Nakajima, T. Nonoyama, T. Kurokawa, O. Ito, H. Ishitobi, J. P. Gong, *Adv. Mater.* **2016**, 28, 4884; c) M. Rikkou-Kalourkoti, E. N. Kitiri, C. S. Patrickios, E. Leontidis, M. Constantinou, G. Constantinides, X. H. Zhang, C. M. Papadakis, *Macromolecules* **2016**, 49, 1731; d) S. Liu, M. Dong, Z. Zhang, G. Fu, *Polym. Adv. Technol.* **2017**, 28, 1065.
- [34] H. Kamata, Y. Akagi, Y. Kayasuga-Kariya, U. I. Chung, T. Sakai, *Science* **2014**, 343, 873.
- [35] a) J. Araki, T. Kataoka, K. Ito, *Soft Matter* **2008**, 4, 245; b) Y. Noda, Y. Hayashi, K. Ito, *J. Appl. Polym. Sci.* **2014**, 131, 40509.
- [36] P. Wang, G. Deng, L. Zhou, Z. Li, Y. Chen, *ACS Macro Lett.* **2017**, 6, 881.
- [37] S. Kondo, T. Hiroi, Y.-S. Han, T.-H. Kim, M. Shibayama, U.-i. Chung, T. Sakai, *Adv. Mater.* **2015**, 27, 7407.
- [38] R. O. Ritchie, *Nat. Mater.* **2011**, 10, 817.
- [39] F. K. Ko, L. Y. Wan, in *Handbook of Properties of Textile and Technical Fibres*, (Ed: A. R. Bunsell), Woodhead Publishing, Cambridge, UK **2018**, pp. 185.
- [40] a) O. Rathore, D. Y. Sogah, *J. Am. Chem. Soc.* **2001**, 123, 5231; b) S. Tanaka, A. Ogura, T. Kaneko, Y. Murata, M. Akashi, **2004**, 37, 1370; c) J. C. Johnson, N. D. Wanasekara, L. T. J. Korley, *Biomacromolecules* **2012**, 13, 1279; d) L. Matolyak, J. Keum, L. T. J. Korley, *Biomacromolecules* **2016**, 17, 3931; e) L. E. Matolyak, C. B. Thompson, B. Li, J. K. Keum, J. E. Cowen, R. S. Tomazin, L. T. J. Korley, *Biomacromolecules* **2018**, 19, 3445; f) D. Jang, C. B. Thompson, S. Chatterjee, L. T. J. Korley, *Mol Syst Des Eng* **2021**, 6, 1003.
- [41] C. B. Thompson, L. T. J. Korley, *Bioconj Chem* **2017**, 28, 1325.
- [42] N. J.-A. Chan, D. Gu, S. Tan, Q. Fu, T. G. Pattison, A. J. O'Connor, G. G. Qiao, *Nat. Commun.* **2020**, 11, 1630.
- [43] S.-W. Kuo, *Hydrogen Bonding in Polymeric Materials*, Wiley-VCH, Weinheim, Germany **2018**.
- [44] S. Ulrich, A. Sadeghpour, R. M. Rossi, N. Bruns, L. F. Boesel, *Macromolecules* **2018**, 51, 5267.
- [45] J. C. Johnson, N. D. Wanasekara, L. T. J. Korley, *J. Mater. Chem. B* **2014**, 2, 2554.
- [46] a) W. K. Surewicz, H. H. Mantsch, D. Chapman, *Biochemistry* **1993**, 32, 389; b) H.-J. Kim, E.-Y. Choi, J.-S. Oh, H.-C. Lee, S.-S. Park, C.-S. Cho, *Biomaterials* **2000**, 21, 131; c) J. Kong, S. Yu, *Acta Biochim. Biophys. Sin.* **2007**, 39, 549; d) S. S. Naik, D. A. Savin, *Macromolecules* **2009**, 42, 7114.
- [47] a) E. Ibarboure, E. Papon, J. Rodríguez-Hernández, *Polymer* **2007**, 48, 3717; b) K. E. Schaefer, P. Keller, T. J. Deming, *Macromolecules* **2006**, 39, 19.
- [48] a) A. Domján, G. Erdödi, M. Wilhelm, M. Neidhöfer, K. Landfester, B. Iván, H. W. Spiess, *Macromolecules* **2003**, 36, 9107; b) D. Zeng, A. Ribbe, R. C. Hayward, *Macromolecules* **2017**, 50, 4668.
- [49] J. C. Lötters, W. Olthuis, P. H. Veltink, P. Bergveld, *J. Microelectromech. Syst.* **1997**, 7, 145.
- [50] E. Ibarboure, J. Rodríguez-Hernández, E. Papon, *J. Polym. Sci., Part A: Polym. Chem.* **2006**, 44, 4668.
- [51] S. Das, I. Yilgor, E. Yilgor, B. Inci, O. Tezgel, F. L. Beyer, G. L. Wilkes, *Polymer* **2007**, 48, 290.
- [52] a) P. J. Rae, E. N. Brown, *Polymer* **2005**, 46, 8128; b) C. R. Siviour, J. L. Jordan, *J. Dyn. Behav. Mater.* **2016**, 2, 15; c) Y. Yu, W. Yang, B. Wang, M. A. Meyers, *Mater. Sci. Eng., C* **2017**, 73, 152; d) Y. Lin, X. Li, X. Chen, M. An, Q. Zhang, D. Wang, W. Chen, P. Yin, L. Meng, L. Li, *Polymer* **2019**, 178, 121579; e) K. Yazawa, A. D. Malay, H. Masunaga, Y. Norma-Rashid, K. Numata, *Commun. Mater.* **2020**, 1, 10; f) E. Sayahi, T. Harizi, S. Msahli, F. Sakli, *J. Nat. Fibers* **2021**, <https://doi.org/10.1080/15440478.2021.1944442>.
- [53] S. Monemian, L. T. J. Korley, *Macromolecules* **2015**, 48, 7146.
- [54] B. S. Lazarus, C. Chadha, A. Velasco-Hogan, J. D. V. Barbosa, I. Jasiuk, M. A. Meyers, *iScience* **2021**, 24, 102798.
- [55] C. Zhang, X. Gou, R. Xiao, *Polym. Test.* **2021**, 95, 107081.
- [56] D. Chen, J. P. Kennedy, A. J. Allen, *J. Macromol. Sci., Part A* **1988**, 25, 389.
- [57] M. Haraszti, E. Toth, B. Ivan, *Chem. Mater.* **2006**, 18, 4952.
- [58] A. Mpoukouvalas, W. Li, R. Graf, K. Koynov, K. Matyjaszewski, *ACS Macro Lett.* **2012**, 2, 23.
- [59] a) R. Katakai, Y. Iizuka, *J. Org. Chem.* **1985**, 50, 715; b) H. Collet, C. Bied, L. Mion, J. Taillades, A. Commeyras, *Tetrahedron Lett.* **1996**, 37, 9043.
- [60] E. Ibarboure, J. Rodríguez-Hernández, E. Papon, *J. Polym. Sci., Part A: Polym. Chem.* **2006**, 44, 4668.